

# Identification of Microaneurysms and Exudates for Early Detection of Diabetic Retinopathy

G. Indira Devi<sup>1</sup>, D. Madhavi<sup>2</sup>

Electronics and Communication Engineering, Anil Neerukonda Institute of Science and Technology, Visakhapatnam, India<sup>1</sup>  
Department of ECE, GIT, GITAM University, Visakhapatnam, India<sup>2</sup>

**Abstract**—Diabetic retinopathy (DR) is a condition that may be a complication of diabetes, and it can damage both the retina and other small blood vessels throughout the body. Microaneurysms (MA's) and Hard exudates (HE's) are two symptoms that occur in the early stage of DR. Accurate and reliable detection of MA's and HE's in color fundus images has great importance for DR screening. Here, a machine learning algorithm has been presented in this paper that detects MA's and HE's in fundus images of the retina. In this research a dynamic thresholding and fuzzy c mean clustering with characteristic feature extraction and different classification techniques are used for detection of MA's and HE's. The performance of system is evaluated by computing the parameters like sensitivity, specificity, accuracy, and precision. The results are compared between different types of classifiers. The Logistic Regression classifier (LRC) performance is good when compared with other classifiers with an accuracy of 94.6% in detection of MA's and 96.2% in detection of HE's.

**Keywords**—Diabetic retinopathy; microaneurysms; hard exudates; SVM; LRC

## I. INTRODUCTION

For the last fifty years, diabetic retinopathy (DR) has been considered the most prevalent cause of blindness. According to epidemiological research conducted in developed nations, DR is one of the four primary causes of vision impairments in the general population. Diabetes damages the blood vessels of the human retina, which is one of the primary causes of visual impairment in DR [1]. In contrast to the nearly non-occurrence of DR in the first five years following a type I diabetes diagnosis, latest is type II which is found in a ratio of 1:5 i.e., one diabetic among five tests has DR at the time of diagnosis. Nonetheless, nearly all type I diabetic patients and two-thirds of type II diabetic individuals have DR symptoms after 15 years.

The most typical signs of DR are abrupt loss of vision, floaters and flashes, and impaired vision. Since DR is a progressive illness, whose severity is dictated by the quantity and variety of lesions visible in the fundus picture, early identification and treatment are essential. The macula, optic disc, and blood vessels that make up a healthy retina are its key constituents; any alterations to these elements are indicative of an eye illness [2]. Non-proliferative DR (NPDR) and proliferative DR (PDR) are the two main phases of DR. NPDR, often referred to as background DR, is a condition in which diabetes destroys the blood vessels in the retina, allowing fluid and blood to seep onto the surface of the retina [3].

Due to the process of leaking the retina gets moist, swollen and finally loses functioning. A variety of retinopathy symptoms, including microaneurysms (MAs), hemorrhages (H), hard-exudates (HE), soft-exudates, or cotton wool spots (CWS), may be present in NPDR. Three phases of non-primary depression (NPDR) are distinguished depending on the severity and number of lesions. These stages included in DR is mild, moderate, and severe which are caused by localized dilatations of thin blood arteries. MAs are the initial indication of NPDR. MAs are tiny, nearly circular, and have a crimson colour H, often known as dot or blot H, is the next indication of DR. Thin vessel or MA walls that are sufficiently weakened may burst and result in H. Larger red lesions are seen in blot haemorrhages, whereas brilliant little red spots are seen in dot haemorrhages. Dot hemorrhages and MAs are occasionally grouped together as a single red lesion type called HMAs. For convenience of viewing, HMA-containing areas in the retinal picture are magnified in Fig. 1.

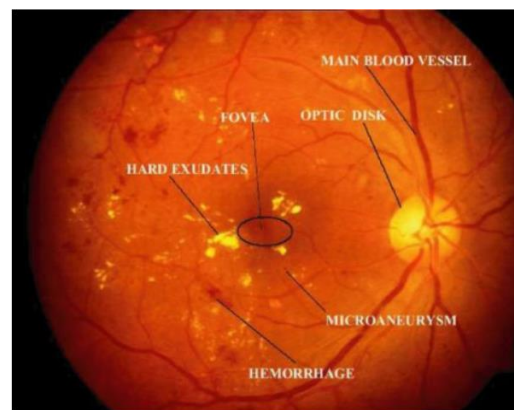


Fig. 1. Retinal fundus image showing MA's and HE's.

When fundus imaging is used to diagnose DR, microaneurysms (MAs) are the initial pathological signs that are identified. They manifest as minute blood bulges that resemble little red spots on the retina. Retinal blood vessels leak due to microaneurysms. Lipids and fluids leak from blood vessels as the condition worsens, forming hard exudates that are yellowish in colour and come in a different type of shapes and sizes. The macula and fovea are the regions in charge of central vision; if exudates accumulate there, the patient may lose or have degraded central vision. In automated DR detection, the Hard Exudates' detection is crucial. To find MAs and HEs, a machine learning method has been created. In this work both MAs and HEs are detected at a time for the given input image. The need of identifying each of them individually

is avoided. So that the treatment can be provided effectively utilizing single process.

The proposal of work is organized in different sections. In Section II a brief overview of existing methods in detection of MA's and HE's is been discussed. The proposed method of extracting features and classification model is discussed in Section III. The experimental findings are evaluated in Section IV and results for identification are given in Section V. Finally, the overall summary is given in Section VI.

## II. RELATED WORK

The diagnosis of DR has made extensive use of computer-aided automated analysis of colour fundus pictures, which is very effective [4]. This might lessen the burden on ophthalmologists and increase the effectiveness of DR screening. Due to the significance of MA for DR diagnosis and the advancement of computer-aided diagnosis (CAD), an increasing number of research on automatic MA detection have been conducted recently. The author in study [5] used the Support Vector Machine (SVM) and Naive Bayesian (NB) classifier to distinguish between red and brilliant lesions; however, they were only able to use one database with 100 images for training and testing. The author in study [6] developed a Random Forest (RF) based approach for the diagnosis of both MA and HM using dynamic shape data, without the need for any prior segmentation of lesions. However, the blood vessel-related lesions were overlooked which resulting in false-negatives (FN) [7].

In research [8], the author suggested filters with various grid sizes combined with MKL, SVM, and filters to cope with false-positives (FP) brought on by tiny blood vessel (BV) segments to detect MA and HM. It was discovered that employing MKL improved performance when compared to using a single grid size, although choosing a larger grid size came with a greater computing cost. To get over the issue of class imbalance, the author in study [9] offered an unsupervised classification approach for MA identification based on sparse principal component analysis (PCA). However, several FPs occur when extracting features. The author in [10] used peak detection and region expansion to obtain MA candidates, and then used K-nearest neighbours (KNN) to identify MA. This led to an e-optha MA database FROC score of 0.273, which is rather low. Singular spectrum analysis (SSA) and a KNN classifier were used by the author in [11] to create a method for MA recognition; however, because there was no subtle or low contrast or blurry-outlined MA, this approach produced multiple false positives (FPs). A few MAs were also overlooked during the selection of candidates.

The author reported a multi-stage automated approach in [12] for identifying longitudinal retinal changes produced by small red colour lesions known as dot HM and MA. The author of [13] employed SVM for classification and local binary pattern (LBP) to extract textural features to detect MA. The author in [14] was able to detect MA by utilizing discriminative dictionary learning (DDL) and multi-feature fusion dictionary learning (MFFDL), respectively. The former mainly relied on the original grayscale feature dictionary, and employing a grayscale feature with single component will

impact the performance since retinal pictures vary greatly in terms of colour, luminance, and contrast.

A key factor in the diagnosis of DR is biomedical engineering. Image processing was used in several studies on diabetic retinopathy to analyze retinal images [15]. In diabetic retinopathy, the GMM classifier was used to automatically detect red lesions [16]. To localizing exudate in the colour fundus picture, morphological operators were employed [17]. Furthermore, a few researchers have looked at the retinal image's hard exudate detection for use in the diagnosis of DR. To detect hard exudate, the retinal picture was subjected to a linear brightness adjustment [18]. In the CIE lab colour model, the hard exudates were identified using k-mean on the colour retinal picture [19]. In DR, the exudates were automatically detected using the wavelet transform [20].

Subsequent research concentrated on deep learning techniques, primarily for image categorization. Convolutional neural networks (CNNs) have the ability to identify picture patches [21] and particular pixels as either exudates or non-exudates [22]. Deep neural networks can be developed from scratch [23] or based on a variety of designs that have been pre-trained on diverse datasets [24] (transfer learning approach). We made the decision to integrate an SVM classifier with transfer learning techniques in order to increase the overall process' efficacy [25].

When it came to DR, there were several methods and procedures for identifying MAs and HEs. The work progressed using morphological processes to identify MA, along with distinctive feature extraction, hessian analysis, and classification algorithms. Dynamic thresholding and fuzzy c mean clustering with distinctive feature extraction are used to identify HE, and classification algorithms are then used.

## III. MATERIAL AND METHODS

### A. Data Utilized

The proposed methodology's execution is carried out utilizing the STARE dataset. There are 400 pictures in this collection, including HEs, MAs, and other diseased features including red lesions of different sizes and forms. The samples images which are available in STATE dataset are shown in Fig. 2.





Fig. 2. Images of stare dataset.

The images of the created database were taken with a Topcon camera, which has a 605 x 700 resolution. Each retinal picture is subjected to an image-based DR detection assessment; however, reference markers for evaluating the approach based on the number of exudates-based assessment are absent. Therefore, an eye expert marked the contours of the lesions of 96 retinal pictures with various features to evaluate the exudates-based effectiveness of the suggested technique. The detection process implemented in this work is shown in Fig. 3.

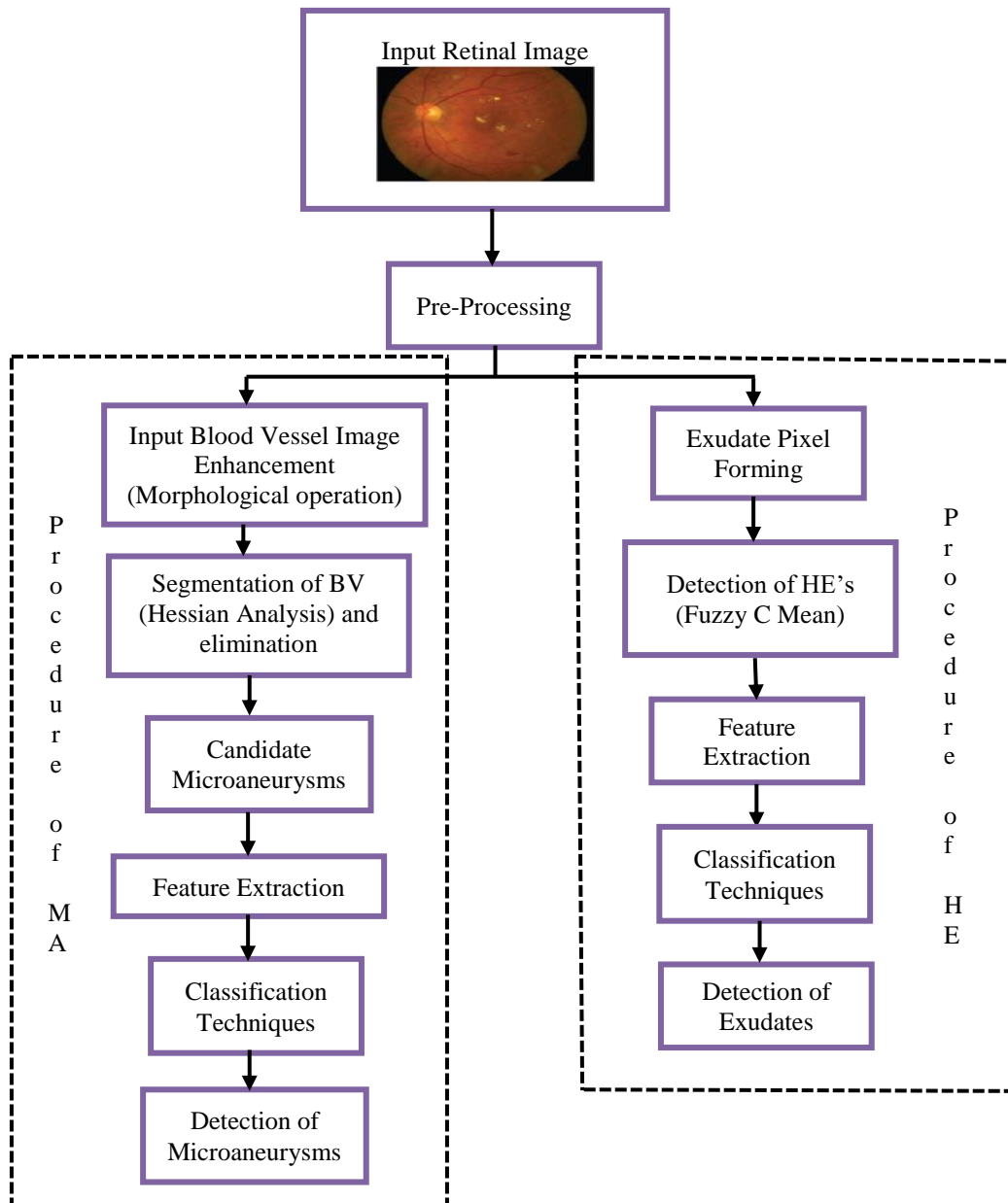


Fig. 3. Process flow of proposed model.

### B. Pre-Processing

The methods in various DR problems are demonstrated using retinal pictures from the STARE dataset. They do, however, differ in brightness and contrast, which are influenced by the surroundings when a fundus camera takes the picture. It causes the complexity of parameter setting and data evaluation, as was previously noted. As a result, the preprocessing portion of the retinal picture is customised to provide appropriate data for additional analysis. The retinal picture is loaded into the system to begin processing. Eq. (1) is then used to adjust the contrast of the retinal picture, producing an image with more clarity than before.

$$C_M(i) = \frac{\max(i) - \min(i)}{\max(i) + \min(i)} \quad (1)$$

The processing is divided into two sections. The first section, the optic disc of retinal image is detected using the algorithm for automatic localization of optic disc in the fundus image [10]. The second one, the retinal image is extracted into three channels (red, green, and blue). The green channel having the complete details of hard exudates is selected for operation. Subsequently, the data is adjusted from 0 to 1 by normalizing function as Eq. (2).

$$N_{(ij)} = \frac{X_{(i,j)} - \min(X)}{\max(X) - \min(X)} \quad (2)$$

The normalized data of the green channel is subtracted by the acquired optic disc.

### C. MA Detection

In the process of MA Detection, initially the blood vessels need to be enhanced and later segmented, finally eliminated.

After eliminating the blood vessels, the remaining area of the fundus images without BV clearly shows the MA's.

1) *Input blood vessel image enhancement*: For the process of enhancing the image of blood vessels morphological filters is been utilized [26]. The contrast between the vessel structure and the backdrop intensity fluctuations is more noticeable. On the other hand, a closer look into vessel intensities may reveal significant alterations that have the potential to negatively impact the extraction process. We have suggested a morphological filter called the modified morph, which has been applied to a normalised green channel picture, to counteract such alterations. The images in the database which contain thickest vessel width is utilized as reference image for performing morphological operations with the range of pixels 1 and 8 for considering the diameter ranges of vessels width. The vessel diameter scale may be modified to account for changes in picture quality.

The morphological operation has been employed to ascertain the disparity among the input image considered and the opened picture. To acquire the inverse picture, first open the image and then close it. The noise sensitivity of the modified morph implementation results in pixel values in an opened image that are always less than or equal to the input values; under these circumstances, the image which are subtracted have low level intensity fluctuations in the data. The

operator 'open' of an image 'I' with structuring element  $S_o$  is given by,

$$I_o = I \circ S_o \quad (3)$$

The operator 'close' function of an image 'I' with structuring element  $S_c$  is given by,

$$I_c = I \cdot S_c \quad (4)$$

Modified morph operation of an image is given by,

$$I_{mod} = I - (I \cdot S_c) \circ S_o \quad (5)$$

The Eq. (5) shows our modified morph operation in which 'I' is the input green channel image while  $S_c$  and  $S_o$  stand for the elements of structuring for closing ( $\cdot$ ) and opening ( $\circ$ ) operators, respectively.

2) *Segmentation of BV and elimination*: Here, the morphological filter is followed in a novel approach by the hessian matrix to improve the quality of the pictures obtained of the thin and broad vessels. For both thin and wide vessel enhancement, we have independently calculated the second derivative of the picture at two distinct scales. The utilisation of a hessian matrix-based technique has facilitated the separation of broad and thin vessels. The focus is on vessels with varying widths, which are determined by analysing the second order derivative at two distinct scales. The hessian matrix's Eigen values and their difference are being utilized to reduce non-vasculature structure and improve contrast. The directed image  $I_i$  and its hessian matrix in the updated coordinates  $Cx'y'$  is found to be,

$$H' = \begin{bmatrix} h_{11} & h_{12} \\ h_{21} & h_{22} \end{bmatrix} = \begin{bmatrix} \frac{\partial^2 I_i}{\partial x'^2} & \frac{\partial^2 I_i}{\partial x' \partial y'} \\ \frac{\partial^2 I_i}{\partial y' \partial x'} & \frac{\partial^2 I_i}{\partial y'^2} \end{bmatrix} \quad (6)$$

Otsu thresholding is applied individually to broad and narrow vessel pictures because applying it to the entire image at once does not yield useful results. So applied a global threshold to the enhanced picture of the broad vessels and then combined it with the enhanced image of the narrow vessels.

Utilising a modified version of Otsu's technique, geometrical objects and undesired noise are suppressed depending on the vessel structure. Otsu's method is often applied locally or globally over the whole picture to determine a threshold for vessel and non-vessel pixel categorization. Otsu threshold is been applied individually to broad and narrow vessel pictures because applying it to the entire image at once does not yield useful results. A global threshold is applied to the enhanced picture of the broad vessels and then combined it with the enhanced image of the narrow vessels. The segmented blood vessel in which one is thin and other is thick vessel is shown in Fig. 4.

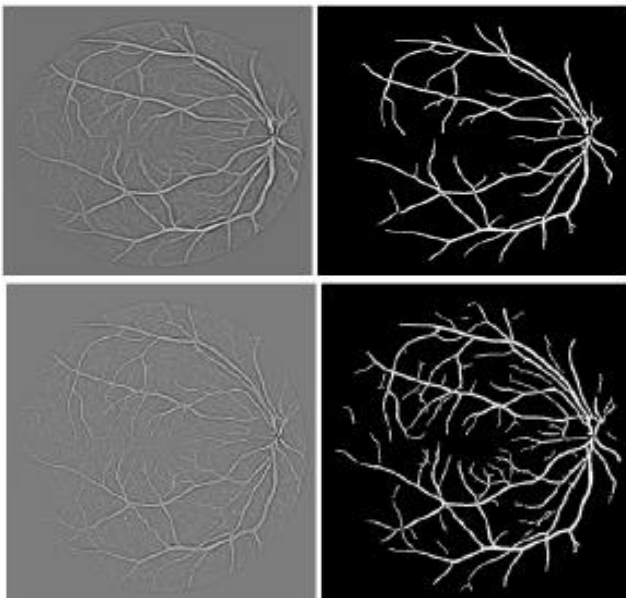


Fig. 4. Thin and thick BVS.

After segmenting the BV's, the blood vessel needs to be eliminated. By eliminating the region of blood vessels, the regions of MA's are easy to extract. The extracted MA region and the morphological filter response on MA region are shown in Fig. 5.

To lessen unwanted noise and geometrical structures according to the design of the vessel, adapted Otsu's technique. Otsu's method is often applied locally or globally over the whole picture to determine a threshold for vessel and non-vessel pixel categorization.

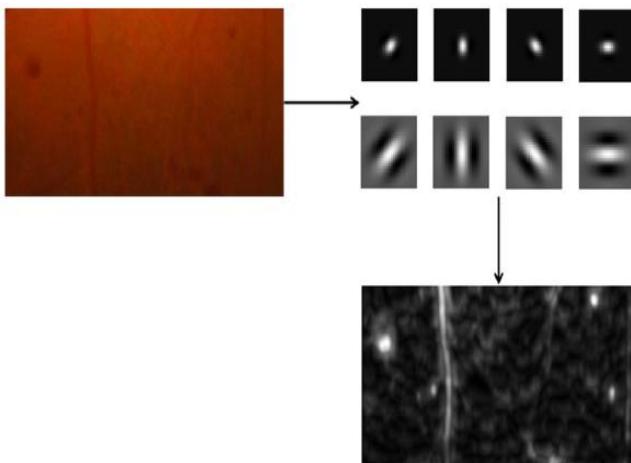


Fig. 5. Slice of Input image with MA region.

3) *Feature extraction*: All prospective objects (regions) that might be regarded as potential MA regions are provided by the candidate MA region extraction step. The set representation for an image 'n' is if it has 'N' probable candidate areas is given as  $n = \{n_1, n_2, n_3, \dots, n_N\}$ . A feature vector with all m characteristics, i.e. for a sample lesion, represents each item or potential lesion region  $n_i$ , which is regarded as a sample for classification and the feature

vector is  $n_i = \{fv_1, fv_2, fv_3, \dots, fv_m\}$  where  $i = 1, 2, \dots, N$ . The area, eccentricity, compactness, aspect ratio, mean and standard deviation, mean gradient, mean gradient magnitude, mean HSV (hue, saturation, and value), entropy, homogeneity, and energy value are the properties that we employ in the system which have been presented. Finally, the features are given to different type of classifiers which are discussed in Section III to identify the detection rate of accuracy.

#### D. HE Detection

1) *Exudates pixel forming*: Retinal pictures must be cleaned of artefacts in order to improve the quality of retinal fundus images for the precise detection of exudates. These artefacts can be caused by a variety of factors, including focus, blur, and improper illumination of the retinal fundus picture. The quality of retinal pictures is declining due to these reasons. Furthermore, poor picture quality may lead to erroneous retinal disease diagnosis. Therefore, improving photos before determining the presence of exudates is a crucial step.

2) *Detection of hard exudates*: There were two primary methods. To segment colour retinal pictures, FCM clustering was first utilised to get the local dynamic threshold of each sub-image. This threshold was then coupled with the global threshold matrix. Subsequently, exudates and non-exudates zones were distinguished using classification algorithms.

a) *FCM for segmentation of retinal image*: The technique of segmenting images using the dynamic threshold in conjunction with the global threshold based on FCM clustering is explained as follows:

i) The retinal picture was split into 'S' sub-images, and each sub-image's pixels were assigned to distinct categories using fuzzy memberships according to the FCM method. The following cost function was minimised by FCM, an iterative optimisation technique:

$$I(A, B) = \sum_{i=1}^n \sum_{s=1}^c (a_{si})^m \|x_i - C_s\|^2 \quad (7)$$

where,  $C_s$  denotes the clustering centre of the kth cluster and  $a_{si}$  denotes the membership of pixel  $x_i$  in the kth cluster. Since the grayscale value was the sole feature utilised for clustering, the midpoint of the line representing the clustering centre was used as the segmentation threshold, and the sub-image threshold was determined by taking the mean of the two clustering centres;

ii) To determine the global threshold and create the global matrix 'G' with the same dimensions as the original picture, all the pixels in the original retinal image were categorised in the same manner as described previously.

iii) A mean filter with a size of  $10 \times 10$  was applied to the dynamic threshold matrix  $T_D$ , which was created by interpolating the thresholds of the individual sub-images into a matrix the same size as the original picture.

iv) The final threshold matrix  $T_h$  was constructed as,

$$T_h = jG + (1 - j)T_D \quad (8)$$

where, the value of 'j' was set to 0.1.

v) The retinal picture and the threshold matrix T were compared to determine the segmentation outcome. Results of retinal imaging segmentation are influenced by the sub-image's size. The FCM clustering results for various sub-image sizes are displayed in Fig. 6. After considering the accuracy of the local threshold as well as the running duration,  $20 \times 35$  pixels was determined to be the most appropriate size for the sub-images.

3) *Feature extraction*: Some notable traits that were frequently employed by eye care professionals to visually identify HE from other forms of lesions were retrieved from each location and used as inputs of classification systems in order to further partition the exudates regions from the exudate's candidates. Area, eccentricity, compactness, aspect ratio, mean and standard deviation, mean gradient, mean gradient magnitude, mean HSV (hue, saturation, and value), entropy, homogeneity, and energy value were among the important characteristics. Lastly, the characteristics are fed into several classifier types—discussed in Section III—to determine the accuracy of the detection rate.

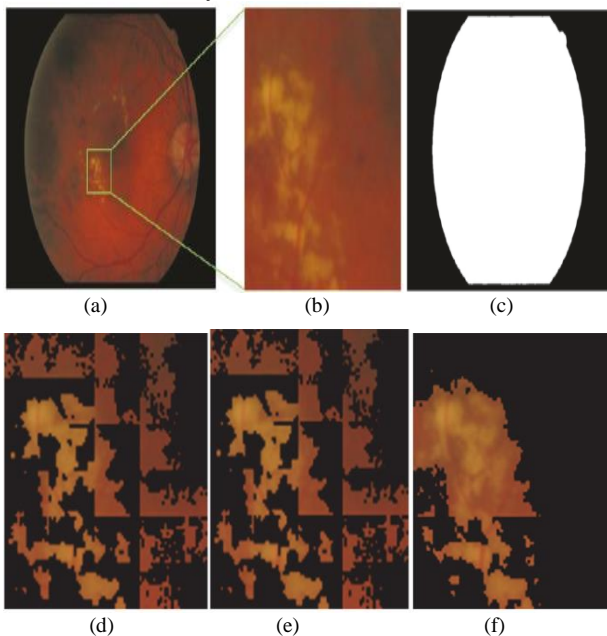


Fig. 6. For different sub-image sizes, the segmentation using FCM clustering. (a) Input image (b) Region of exudates (c) FCM segmented output (d) Segmentation with a size of  $10 \times 15$ . (e) with  $20 \times 35$  pixels. (f) With  $50 \times 60$  pixels.

### E. Classification Techniques

Following the extraction of the features, five classifiers—DT, RF, SVM, KNN, and LR—are used to begin the classification process. Adaptive threshold algorithms are used in both methods to improve pictures, with 94.6 and 96.2 accuracy levels for MA and HE identification, respectively.

1) *Decision Tree (DT)*: DT is a popular hierarchical machine learning technique for prediction that uses a model of decisions and possible outcomes that resembles a tree. Every branch of DT reflects the test results, every internal node and

that is not a leaf node evaluates an attribute, and every leaf node or terminal node specifies the label class.

2) *Random Forest (RF)*: A Random Forest Classifier, which gathers data from MAs and divides it into two likely classes healthy and unhealthy is the third stage. This method operates in a manner akin to that of the decision tree algorithm. This method discovers the optimal answer by compiling all the decision tree predictions. Every tree is dependent on the collection of random features.

3) *K-Nearest Neighbour (KNN)*: KNN is a supervised machine learning technique that predicts the values of new data items by using "feature similarity". In the classification phase, the unlabelled sample is categorised by designating the class label depending on which of the k training samples that are closest to the query point—where k is a predetermined constant—is the most common. In the training phase, this is accomplished by storing the feature vectors and class labels of the training samples.

4) *Support Vector Machine (SVM)*: SVM is a supervised machine learning algorithm that may be applied to problems related to regression and classification. This method constructs a hyperplane (or a group of hyper-planes) in a high- or infinite-dimensional space to determine the best boundary between the potential outputs. Finding a hyperplane that maximises the isolation of data points from possible groupings is the aim in n-dimensional space. SVMs can manage very large feature spaces because they use over-fitting avoidance, which is independent of feature count.

5) *Logistic Regression (LR)*: For classification situations where the goal is to predict the chance that a given instance will belong to a specific class, supervised machine learning techniques termed logistic regression are typically utilised. The word used to describe the classification techniques that use it is logistic regression. The outcome of a categorical dependent variable is predicted using logistic regression. The outcome must thus be a discrete or category value. It gives the probabilistic values that lie between 0 and 1, as opposed to the exact values of 0 and 1. It might be true or false, 0 or 1, yes or no, etc. It is quite like linear regression, except for how they are used.

Regression issues are solved using linear regression, and classification challenges are resolved using logistic regression. We fit a logistic function with a "S" shape that predicts two maximum values, 0 and 1, in lieu of fitting a regression line in LR. The logistic function's curve indicates a number of potential outcomes, such as the presence of cancerous cells and the relationship between a mouse's weight and fatness.

#### Algorithm for Training:

This section outlines the fundamental procedures for creating a picture (training set) and a collection of targets, as well as the processes we do in the order listed below:

For  $i = 1$ , to the number of training images,

Obtain the  $i^{\text{th}}$  image from the database,

Apply to preprocess and extract the features,

Stack the feature results to the training image array,

Assign a target class based on the severity of the dataset

Train classifiers: The following classifiers are picked to carry out the actions, and this sub segment specifies the necessary procedures to train the chosen classifier:

- Train the DT classifier,
- Train the RF classifier,
- Train the KNN classifier,
- Train the SVM classifier, and
- Train the LR classifier.

Algorithm for Testing:

This section outlines the general processing procedures to forecast the outcomes using the provided classifier's feature extraction technique and the subsequent steps we do in that order:

- Step1. Obtain the desired test image,
- Step2. Apply image pre-processing and extract the features,
- Step3. Predict the DT classifier features
- Step4. Predict the RF classifier features
- Step5. Predict the KNN classifier features,
- Step6. Predict the SVM classifier features
- Step7. Predict the LR classifier features,
- Step8. Obtain the model of prediction results.

#### IV. EXPERIMENTAL FINDINGS

To assess the effectiveness of the suggested detection framework, retinal pictures from the publicly accessible STARE dataset were analysed in this study. Expertly segmented retinal pictures constitute the dataset, which is often regarded as the gold standard for comparison. The 40 and 20 retinal pictures in the STARE datasets, respectively, are divided into training and test sets. The suggested methodology has been used to evaluate performance using 20 test photos from the STARE dataset. Our suggested framework's trials were all carried out using the aid of the software programme MATLAB 2021a.

The parameters evaluated to show the performance of proposed detection model are sensitivity, specificity, precision, and accuracy. The finding of accuracy is based on true positive, true negative, false positive and false negative values. Here the values signify how effective the MA's and HE's are detected. The classification needs to be correct to achieve correct values. The entire performance of segmentation is shown by accuracy. Specificity measures the identification of pixels with negative values, whereas sensitivity represents the ability of detecting pixels with positive values. The following formulae provide the findings, which are displayed in Tables I and II.

$$Sensitivity = \frac{TP}{TP+FN} \quad (9)$$

$$Specificity = \frac{TN}{TN+FN} \quad (10)$$

$$Precision = \frac{TP}{TP+FP} \quad (11)$$

$$Accuracy = \frac{TP+TN}{TP+TN+FP+FN} \quad (12)$$

#### V. RESULTS FOR MA'S IDENTIFICATION

TABLE I. RESULTS FOR MA'S IDENTIFICATION

Classification Technique	Accuracy (%)	Sensitivity (%)	Specificity (%)	Precision (%)
Decision Tree	83.4	85.4	84.7	87.5
Random Forest	87.6	88.3	87.2	89.6
KNN	93.7	94.2	94.8	95.2
SVM	94.2	95.7	94.9	96.4
Logistic Regression	94.6	96.5	96.2	97.6

TABLE II. RESULTS FOR HE'S IDENTIFICATION

Technique	Accuracy (%)	Sensitivity (%)	Specificity (%)	Precision (%)
Math Morph [26]	0.92	0.89	0.91	-
Deep CNN [27]	0.69	0.64	0.88	-
2 step CNN [28]	-	0.77	-	-
MSRNet [29]	-	0.71	-	-
Decision Tree	84.6	86.5	85.2	88.2
Random Forest	87.2	89.1	88.6	90.3
KNN	93.1	95.3	95.1	96.7
SVM	95.2	96.4	95.9	97.8
Logistic Regression	96.2	97.6	97.2	98.4

TABLE III. OVERALL ACCURACY OBTAINED USING PROPOSED MODEL

Classification Technique	MA's and HE's Accuracy (%)
Decision Tree	84.0
Random Forest	87.4
KNN	93.8
SVM	94.7
Logistic Regression	95.3

The discussion of Table III is all about the overall rate of accuracy obtained by various machine learning techniques in detection of MAs and HEs for the given STARE dataset. The LR classification achieved higher rate of accuracy with 95.3% when compared to techniques like DT, RF, KNN, and SVM. The classifiers performance may be more accurately assessed using the receiver operating characteristic (ROC) curve and is shown in Fig. 7.

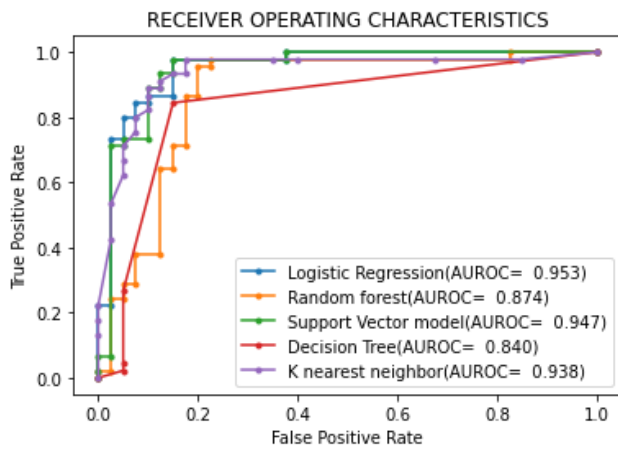


Fig. 7. Over-all ROC in detection of MA's and HE's.

According to this analysis, there are significantly fewer MAs and HEs in regions that are candidates than there are non-MAs and non-HEs. The ROC curve and corresponding AUC of MA detection results on stare database achieved by five classifiers (Decision tree, Random-forest, KNN, SVM and LR) are shown in Fig. 7. Fig. 8 describes the overall training accuracy of the six machine learning classifiers.

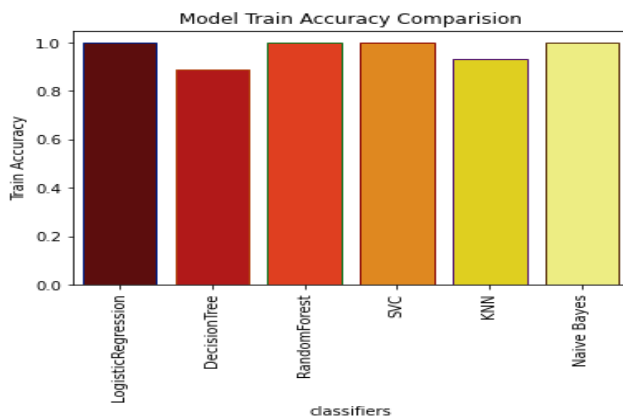


Fig. 8. Overall training accuracy of proposed model.

## VI. CONCLUSION

The detection of MAs and HEs to identify the early stage of DR is displayed in this article. The suggested model consists of three main stages i.e., preprocessing, extraction of features and classification. In terms of accuracy, sensitivity, and specificity, respectively, the classifier logistic regression outperformed the other classification methods including DT, RFC, SVM, and KNN. However, because the preprocessing and extraction of feature steps are the only ones that control the whole system, the results are always a compromise between the necessary parameters. The suggested approach has been tested on databases such as STARE and evaluated using performance metrics as discussed in results. The Logistic Regression classifier (LRC) performance is good when compared with other classifiers with an accuracy of 94.6% in detection of MA's and 96.2% in detection of HE's. In future, research endeavors might involve integrating deep learning techniques

into the machine learning algorithm and contrasting the outcomes with the ongoing study.

## REFERENCES

- [1] R.Klein,B.E.K.Klein,S.E.Moss,Visualimpairmentindiabetes,Ophthalmology 91,1-9, 1994.
- [2] Melville A, Richardson R, McIntosh A, O'Keeffe C, Mason J, Peters J, Hutchinson A. Complications of diabetes: screening for retinopathy and management of foot ulcers. Qual Health Care. 2000 Jun;9(2):137-41. doi: 10.1136/qhc.9.2.137.
- [3] P.C.Ronald,T.K.Peng, A Textbook of Clinical Ophthalmology:A Practical Guide to Disorders of the Eyes and Their Management,3rd,World Scientific Publishing Company,Singapore,2003.
- [4] Chaturvedi SS, Gupta K, Ninawe V, Prasad PS. Advances in computer-aided diagnosis of diabetic retinopathy. arXiv-prints, 1909-09853 (2019). 1909.09853.
- [5] Saha R, Chowdhury AR, Banerjee S. Diabetic retinopathy related lesions detection and classification using machinelearning technology. 2016;734-45.
- [6] Seoud L, Hurtut T, Chelbi J, Cheriet F, Langlois JMP. Red lesion detection using dynamic shape features for diabeticretinopathy screening. IEEE Trans Med Imag. 2016;35(4):1116-26.
- [7] Biyani RS, Patre BM. Algorithms for red lesion detection in diabetic retinopathy: a review. Biomed Pharmacother.2018;107:681-8.
- [8] Srivastava R, Duan L, Wong DWK, Liu J, Wong TY. Detecting retinal microaneurysms and hemorrhages with robustness to the presence of blood vessels. Comput Methods Progr Biomed. 2016;138:83-91.
- [9] Zhou W, Wu C, Chen D, Yi Y, Du W. Automatic microaneurysm detection using the sparse principal component analysis-based unsupervised classification method. IEEE Access. 2017;5:2563-72.
- [10] Wu B, Zhu W, Shi F, Zhu S, Chen X. Automatic detection of microaneurysms in retinal fundus images. Comput MedImaging Graph. 2017;55:106-12.
- [11] Wang S, Tang HL, Turk LA, Hu Y, Sanei S, Saleh GM, Peto T. Localizing microaneurysms in fundus images through singular spectrum analysis. IEEE Trans Biomed Eng. 2017;64(5):990-1002.
- [12] Adal KM, Sidibe D, Ali S, Chaum E, Karnowski TP, Meriaudeau F. Automated detection of microaneurysms using scale-adapted blob analysis and semi-supervised learning. Comput Methods Progr Biomed. 2014;114(1):1-10.
- [13] Derwin DJ, Selvi ST, Singh OJ. Secondary observer system for detection of microaneurysms in fundus images using texture descriptors. J Digit Imaging. 2019;1-9.
- [14] Javidi M, Pourreza HR, Harati A. Vessel segmentation and microaneurysm detection using discriminative dictionary learning and sparse representation. Comput Methods Progr Biomed. 2017;139:93-108.
- [15] M. Preethi. and R. Vanithamani., "Review of retinal blood vesseldetection methods for automated diagnosis of Diabetic Retinopathy,"IEEE-International Conference On Advances In Engineering,Science And Management (ICAESM -2012), Nagapattinam,Tamil Nadu, 2012,pp. 262-265.
- [16] V. Saravanan, B. Venkatalakshmi and V. Rajendran, "Automated redlesion detection in diabetic retinopathy," 2013 IEEE Conference onInformation & Communication Technologies, Thuckalay, TamilNadu, India, 2013, pp. 236-239.
- [17] M. Akter, M. S. Uddin, and M. H. Khan, "Morphology-basedExudates Detection from Color Fundus Images in Diabetic Retinopathy," International Conference on Electrical Engineering andInformation & Communication Technology (ICEEICT), 2014, pp. 1-4.
- [18] A.K. Dixit and P. Prabhakar, "Hard Exudate Detection Using LinearBrightness Method", 4th International Conference on Recent Trendson Electronics, Information, Communication & Technology(RTEICT), 2019, pp. 980-984.
- [19] G. G. Rajput and P. N. Patil, "Detection and Classification ofExudates Using K-Means Clustering in Color Retinal Images," 2014Fifth

- International Conference on Signal and Image Processing, Bangalore, India, 2014, pp. 126-130.
- [20] P. Kokare, "Wavelet based automatic exudates detection in diabetic retinopathy," 2017 International Conference on Wireless Communications, Signal Processing and Networking (WiSPNET), Chennai, 2017, pp. 1022-1025.
- [21] Auccahuasi, W. *et al.* Recognition of hard exudates using deep learning. *Procedia Comput. Sci.* **167**, 2343–2353 (2020).
- [22] Prentasic, P. & Loncaric, S. Detection of exudates in fundus photographs using deep neural networks and anatomical landmark detection fusion. *Comput. Methods Progr. Biomed.* **137**, 281–292 (2016).
- [23] Sadek, I., Elawady, M. & Shabayek, A. E. R. Automatic classification of bright retinal lesions via deep network features. In *Computer Vision and Pattern Recognition* (2017).
- [24] Abbasi-Sureshjani, S., Dashtbozorg, B., Romeny, B. M. H. & Fleuret, F. Boosted exudate segmentation in retinal images using residual nets. In *Fetal, Infant and Ophthalmic Medical Image Analysis International Workshop, FIFI 2017 and 4th International Workshop OMIA 2017 Held in Conjunction with MICCAI 2017, Proceedings*, 210–218. (Springer, 2017).
- [25] Khojasteh, P. *et al.* Exudate detection in fundus images using deep-learnable features. *Comput. Biol. Med.* **104**, 62–69 (2019).
- [26] Joshi, S.; Karule, P. Mathematical morphology for microaneurysm detection in fundus images. *Eur. J. Ophthalmol.* 2020, 30, 1135–1142.
- [27] Harangi, B.; Toth, J.; Hajdu, A. Fusion of Deep Convolutional Neural Networks for Microaneurysm Detection in Color Fundus Images. In *Proceedings of the 2018 40th Annual International Conference of the IEEE Engineering in Medicine and Biology Society (EMBC)*, Honolulu, HI, USA, 18–21 July 2018.
- [28] Eftekhari, N.; Pourreza, H.-R.; Masoudi, M.; Ghiasi-Shirazi, K.; Saeedi, E. Microaneurysm detection in fundus images using a two-step convolutional neural network. *Biomed. Eng. Online* 2019, 18, 67.
- [29] Xia, H.; Lan, Y.; Song, S.; Li, H. A multi-scale segmentation-to-classification network for tiny microaneurysm detection in fundus images. *Knowl.-Based Syst.* 2021, 226, 107140.